

# Adsorption and dissociation of molecular hydrogen on orthorhombic $\beta$ -Mo<sub>2</sub>C and cubic $\delta$ -MoC (001) surfaces

Sergio Posada-Pérez<sup>a</sup>, Francesc Viñes<sup>a,\*</sup>, Rosendo Valero<sup>a</sup>,

José A. Rodríguez<sup>b</sup>, Francesc Illas<sup>a</sup>

<sup>a</sup> *Departament de Ciència de Materials i Química Física & Institut de Química Teòrica i Computacional (IQTCUB), Universitat de Barcelona, c/ Martí i Franquès 1, 08028 Barcelona, Spain*

<sup>b</sup> *Chemistry Department, Brookhaven National Laboratory, Upton, NY 11973, USA*

## Abstract

Molybdenum carbides are increasingly used in heterogeneously catalyzed hydrogenation reactions, which imply the adsorption and dissociation of molecular hydrogen. Here a systematic density functional theory based study, including or excluding dispersion terms, concerning the interaction and stability of H<sub>2</sub> with cubic  $\delta$ -MoC(001) and orthorhombic  $\beta$ -Mo<sub>2</sub>C(001) surfaces is presented. In the latter case the two possible C or Mo terminations are considered. In addition, different situations for the H covered surfaces are examined. Computational results including dispersive forces predict as essentially spontaneous dissociation of H<sub>2</sub> on  $\beta$ -Mo<sub>2</sub>C(001) independently of the surface termination, whereas on  $\delta$ -MoC(001) molecular hydrogen dissociation implies a small but noticeable energy barrier. Furthermore, the *ab initio* thermodynamics formalism has been used to compare the stability of different H coverages. Finally, core level binding energies and vibrational frequencies are presented with the aim to assist the interpretation of yet unavailable data from X-ray photoelectron and infrared spectroscopies.

\*Corresponding author: [francesc.vines@ub.edu](mailto:francesc.vines@ub.edu)

**Keywords:** Density functional calculations • Molybdenum carbides • H<sub>2</sub> dissociation • *Ab initio* thermodynamics • IR spectroscopy • Core level shifts

## 1. Introduction

The pioneering work of Levy and Boudart [1] showing that, for a variety of reactions, the catalytic activity of WC is similar or even better than that of platinum, triggered a number of studies dealing with reactions catalyzed by early transition metal carbides (TMCs) [2-5]. The interest on the catalytic properties of TMCs surfaces has been accompanied by a significant number of surface science studies [3,6,7]. Nevertheless, one must realize that, in some cases, preparing well-defined single crystal surfaces can be extremely difficult. This is for instance the case of  $\delta$ -MoC, which, due to the complex phase diagram of MoC [7], is usually found in the form of polycrystalline samples. It is important to point out that, in addition to their remarkable catalytic [8] and electrocatalytic [9] activities, TMCs are widely used in different applications due to their appealing chemical properties such as extreme hardness [10], excellent electric and thermal conductivities [2], and high melting points [11].

In the past ten years the catalytic activity of the different available TMCs has been investigated for several reactions, either as the active phase or as support [12-14]. Owing to their activity and the fact that they do not require special conditions for their synthesis [15], Mo carbides have stood out among other TMCs. Very recently it has been shown that the interaction of ethylene with  $\delta$ -MoC(001) and Pt(111) exhibits a similar adsorption energy [16], further reinforcing the idea that early TMCs exhibit chemical features of late transition metals. On the other hand, Mo<sub>2</sub>C phases have been proposed as alternative to commercial catalyst for water gas shift reaction (WGS) [17] and Pt/Mo<sub>2</sub>C based catalyst also display very high rates for WGS [18]. Mo<sub>2</sub>C is also active for the hydrogenation of dimethyl oxalate towards ethanol [19], the hydrodeoxygenation of butiric acid [20], the formic acid decomposition to CO and H<sub>2</sub> [21], CO<sub>2</sub> reduction [4,22], and its conversion to CO, CH<sub>4</sub>, methanol, or ethanol [23-25], although a very recent study showed that MoC, Cu/MoC, and Au/MoC are more selective and stable catalysts than Mo<sub>2</sub>C, Cu/Mo<sub>2</sub>C, and Au/Mo<sub>2</sub>C for CO<sub>2</sub> conversion [26]. Furthermore, steam reforming catalysis has been recently theoretically tackled using  $\delta$ -MoC and  $\beta$ -Mo<sub>2</sub>C [27].

Many of these chemical reactions involve hydrogenation and/or dehydrogenation steps. Hence, the relative stability of the different phases of the Mo carbides in absence/presence of H<sub>2</sub> is also an important issue to evaluate their possible use in hydrogenation reactions. Likewise, the study of the H<sub>2</sub> adsorption/desorption and

H<sub>2</sub> dissociation/formation elementary steps is important since these are common and determinant ones and, therefore, understanding the molecular mechanisms involved in these pathways is essential to reach a complete picture of the underlying chemistry. The objective of the present study is precisely to carry out a systematic theoretical work about the interaction of H<sub>2</sub> with (001) surfaces of orthorhombic Mo<sub>2</sub>C and cubic MoC carbides. This work also aims to complement a recent study published by Wang and coworkers [28] where the stability of different terminations of orthorhombic Mo<sub>2</sub>C at different H coverages is exhaustively studied within the framework of *ab initio* thermodynamics [29,30]. We report these results also including the stability of  $\delta$ -MoC and, in addition, analyzing H<sub>2</sub> adsorption and its dissociation/formation providing as well estimates of C 1s core level binding energy shifts and vibrational fingerprints to assist the interpretation of forthcoming data from X-ray photoelectron (XPS) and infrared spectroscopies (IR).

## 2. Computational Details

First of all, and in order to avoid any possible misunderstanding arising from the different notations used in the literature for molybdenum carbides, it is necessary to highlight that here we follow the notation convention defined by the joint committee on powder diffraction standards (JCPDS) data files [31]. This notation is the same used in our previous work [32] and also by others [33]. So, hexagonal and orthorhombic Mo<sub>2</sub>C crystal structures are denoted as  $\alpha$ -Mo<sub>2</sub>C and  $\beta$ -Mo<sub>2</sub>C, respectively. Note, however, that some authors in the literature refer to orthorhombic Mo<sub>2</sub>C as  $\alpha$ -Mo<sub>2</sub>C [34-36], following an early definition by Christensen [37]. In the case of MoC, the cubic phase is always referred to as  $\delta$ -MoC. The space group for  $\beta$ -Mo<sub>2</sub>C is *Pbcn* [38] and for cubic  $\delta$ -MoC is *Fm $\bar{3}m$* . In all cases, the (001) surface is considered and represented by suitable slab models. These contain four atomic layers and involve a (2 $\times$ 2) supercell. In the case of  $\beta$ -Mo<sub>2</sub>C, two possible terminations are possible for the (001) surface exposing either C or Mo atoms to the vacuum. Hereafter these surfaces are referred to as  $\beta$ -C and  $\beta$ -Mo, respectively.

The periodic density functional calculations (DFT) were performed using the Perdew-Burke-Ernzerhof (PBE) exchange-correlation functional [39], neglecting or including van der Waals interactions. In the latter case, the method proposed by Grimme (D2) [40] has been chosen. The electronic density of the valence electrons is expanded in a plane-wave basis set and the effect caused by the core electrons on those

in the valence region is described by the projected augmented wave (PAW) method of Blöch [41] as implemented by Kresse and Joubert [42]. Numerical integration in the reciprocal space was carried out using  $3 \times 3 \times 1$  and  $5 \times 5 \times 1$  Monkhorst-Pack  $\mathbf{k}$ -points grids [43] for  $\delta$ -MoC and  $\beta$ -Mo<sub>2</sub>C slabs, respectively. These settings are as in our previous work, where the stability of different surfaces of these carbides has been studied in detail, finding them suited to provide highly-accurate results [32]. An electronic relaxation criterion of  $10^{-5}$  eV was used, and the atomic positions were allowed to relax until forces acting on atoms were always smaller than  $0.01 \text{ eV } \text{\AA}^{-1}$ . Transition state structures have been located using the Dimer method [44] and characterized *via* frequency analysis of the modes related to the adsorbate expand the description presented in previous works [45]. In all cases calculations have been carried out by fully relaxing the two outermost atomic layers whereas the two bottommost were fixed as in the bulk to provide an adequate environment to the atoms in the surface region. The energies have been corrected using zero point energy (ZPE) taking into account the vibrations of the gas phase and the adsorbates. All DFT calculations were carried out using the VASP code [46]. The adsorption site nomenclature is detailed in Refs. [23] and [47].

Furthermore, we used the *ab initio* thermodynamics formalism proposed by Reuter and Scheffler [29,30] to estimate the surface free energy after H adsorption ( $\gamma^{\text{cover}}$ ) —Gibbs adsorption energy per surface area— at different hydrogen coverages ( $N$ ) and as a function of pressure ( $p$ ) and temperature ( $T$ ). The  $\gamma^{\text{cover}}$  can be calculated as the sum of the surface free energy of the clean surface ( $\gamma^{\text{clean}}$ ) plus the Gibbs free energy related with the adsorption of H atoms ( $\gamma^{\text{ads}}$ ), both of them normalized per surface area, following Eq. 1.

$$\gamma^{\text{cover}}(T, p, N) = \gamma^{\text{clean}}(T, p) + \gamma^{\text{ads}}(T, p, N) \quad (1)$$

Following Reuter and Scheffler [29,30], the surface free energy of a clean surface as function of  $p$  and  $T$  can be obtained using Eq. 2:

$$\gamma^{\text{clean}}(T, p) = \frac{1}{A} [G^{\text{clean}}(T, p) - \sum_i N_i \mu_i(T, p)] \quad (2)$$

where  $G^{clean}$  is the Gibbs free energy of the surface,  $\mu_i(T, p)$  is the chemical potential of the  $i$  species which form the solid surface,  $N_i$  is the number of atoms of element  $i$ , and  $A$  is the total surface area. For  $\text{Mo}_x\text{C}$  carbides surfaces, one can adapt Eq. 2 as shown on Eq. 3.

$$\gamma^{clean}(T, p) = \frac{1}{A} [G_{\text{Mo}_x\text{C}}^{slab} - N_C \mu_C(T, p) - N_{\text{Mo}} \mu_{\text{Mo}}(T, p)] \quad (3)$$

where  $G_{\text{Mo}_x\text{C}}^{slab}$  is the Gibbs free energy of  $\delta\text{-MoC}$  or  $\beta\text{-Mo}_2\text{C}$  surfaces and  $\mu_C$  and  $\mu_{\text{Mo}}$  are the chemical potentials of C and Mo atoms, normally obtained using graphite and Mo bulk references, respectively [28,48]. The  $N_C$  and  $N_{\text{Mo}}$  terms are the number of C and Mo atoms on the surfaces. Here, one has to point out that the slab models used in the present work contain four layers, two of them fixed and the two outermost relaxed. This fact leads to different energy values depending on the surface termination or require using a different model to estimate the  $\gamma^{clean}$  term. For this reason, we approximate  $\gamma^{clean}$  as the surface energy predicted in previous works [32]. In the case of Mo- and C-terminated  $\beta\text{-Mo}_2\text{C}$  surfaces we used instead the cleavage energies computed as proposed by Moreira and coworkers [49]. This is because estimating the surface energy of slabs with two differently terminated surfaces is cumbersome [50]. Note that by using these surface energy values, the chemical potential of C and Mo atoms does not need to be taken into account. Instead, the calculated values are referred to MoC and  $\text{Mo}_2\text{C}$  bulk materials.

Aside, the adsorption Gibbs free energy [ $\gamma^{ads}(T, p, N)$ ] can be estimated as in Eq. 4.

$$\gamma^{ads}(T, p, N_H) = \frac{1}{A} [G^{cover}(T, p, N_H) - G_{\text{Mo}_x\text{C}}^{slab}(T, p) - G^{H_2}(T, p)] \quad (4)$$

where  $G^{cover}(T, p, N_H)$  is the Gibbs energy of the H covered surface at  $T$ ,  $p$ , and containing  $N_H$  hydrogen atoms, and  $G^{H_2}(T, p)$  the Gibbs energy of the  $\text{H}_2$  molecule also at  $T$  and  $p$ . In addition, the  $G^{cover}(T, p, N_H)$  and  $G_{\text{Mo}_x\text{C}}^{slab}(T, p)$  terms can be obtained from the DFT energy of the covered and clean slabs since

$$G^{cover}(T, p, N_H) = (E^{cover} - TS^{cover} + pV) \quad (5)$$

$$G_{\text{Mo}_x\text{C}}^{slab}(T, p) = (E_{\text{Mo}_x\text{C}}^{slab} - TS_{\text{Mo}_x\text{C}}^{slab} + pV) \quad (6)$$

where  $E^{cover}$  and  $E_{Mo_xC}^{slab}$  are the total energy of the systems (covered and clean) obtained from the corresponding DFT based calculations ( $E^{total}$ ) plus the zero point vibrational energy ( $E^0$ ),  $S^{cover}$  and  $S_{Mo_xC}^{slab}$  are the corresponding entropy values, and  $pV$  is the pressure-volume term. Both entropy and  $pV$  terms are usually neglected. Note, in fact, that for a cell dimension of  $10 \times 10 \times 10$  Å and an external pressure of at  $10^5$  Pa, the contribution of  $pV$  term is 1 meV, and a similar argument applies to the entropy term [29,30]. Therefore, Gibbs free energy of clean and H covered surfaces are represented by the total energy of clean ( $E^{clean}$ ) and covered ( $E^{cover}$ ) surfaces obtained by DFT calculations, whereas the Gibbs energy for the gas takes into account all thermodynamic contributions. With these approximations one can estimate the adsorption surface free energy ( $\gamma^{ads}$ ) as in Eq. 7.

$$\gamma^{ads}(p, T, N_H) \frac{1}{A} \left[ E^{cover} - E_{Mo_xC}^{slab} - N_H \left( \frac{E_{H_2}}{2} + \frac{E_{H_2}^{ZPE}}{2} + \Delta\mu_{0_{H_2}} + k_B T \ln \frac{p}{p_0} \right) \right] \quad (7)$$

where  $E_{H_2}$  is the DFT total energy of  $H_2$  molecule in vacuum,  $E_{H_2}^{ZPE}$  is its zero point energy correction,  $k_B$  is the Boltzmann constant,  $p$  is the working pressure and  $\Delta\mu_{0_{H_2}}$  is the chemical potential of  $H_2$  calculated as in Eq. 8.

$$\Delta\mu_{0_{H_2}} = -\frac{1}{2} k_B T \ln Q_{Total} \quad (8)$$

where  $Q_{Total}$  is the sum of the electronic, rotational, translational, and vibrational partition functions of the gas phase  $H_2$  molecule. Note that the definition in Eq. 8 implicitly contains a dependence on  $p$  and  $T$ .

Regarding to the predictions concerning core level binding energy shifts ( $\Delta CLBE$ ), two different approximations are often used in theoretical calculations using either Hartree-Fock (HF) [51-53] or DFT based approaches [54-56]. On one hand, one has the initial state approximation, which computes CLBEs without taking into account the electron density relaxation effect upon one core electron ionization. Here, a ground state calculation is necessary without considering the core hole effect. The CLBE in the initial state approach requires computing the energy of the core hole ionized system using the density of the neutral molecule. It has been also claimed that initial state values for CLBEs can be derived from the Kohn-Sham eigenvalues. This has, however, proven to be incorrect although Kohn-Sham eigenvalues nicely follow the trends of

$\Delta$ CLBEs with respect to a given reference [56]. Here,  $\Delta$ CLBEs for the C(1s) of the MoC and Mo<sub>2</sub>C surfaces at different hydrogen coverage have been computed relying on the PAW eigenvalues energy ( $E_C$ ) computed with respect to the Fermi level ( $E_F$ ), as in Eq. 9.

$$BE = E_F - E_C \quad (9)$$

On the other hand, a more accurate estimate of CLBEs or  $\Delta$ CLBEs requires taking into account the relaxation of the core and valence electron density in response to the creation of the core hole; this is usually referred to as final state contribution and CLBEs including the final state contribution are broadly described final state approaches. Strictly speaking, to obtain the final state contribution it is necessary to carry out variational calculations for the system in the ground state and for the system with a core hole. The procedure is usually referred to as  $\Delta$ SCF no matter whether the SCF calculation is of HF or DFT type [56]. For periodic systems, where the core electrons are often described with a pseudopotential,  $\Delta$ SCF calculations are far from being straightforward and further simplifications are usually made.

One way is to mimic a core hole ionization by a corresponding core excited pseudopotential generated on-the-fly and the missing electron added to the valence band to keep the system neutrality. These approximations may cause errors in absolute values of the calculated CLBEs and thus only  $\Delta$ CLBE relative shifts are meaningful as in the case of initial state approximation [56]. Kölher and Kresse argued that, in this approximation, the shifts between the bulk and surface are expected to agree with the experiments because, in metallic systems, the valence electrons rapidly screen the core hole [57]. Therefore, to avoid the above described problem related to the use of  $\Delta$ SCF calculations in periodic systems, we rely on initial state values only and obtain  $\Delta$ CLBES relative to the bulk C(1s) CLBE of  $\delta$ -MoC and of  $\beta$ -Mo<sub>2</sub>C. Therefore,  $\Delta$ CLBE values have been computed as in Eq. 10,

$$\Delta\text{CLBE} = (E_F - E_C) - (E_{F-\text{Bulk}} - E_{C-\text{Bulk}}) \quad (10)$$

where  $E_{F-\text{Bulk}}$  is the Fermi level of the bulk carbide and  $E_{C-\text{Bulk}}$  stands for the Kohn-Sham eigenvalue of the core state. The bulk systems have been calculated using the same criteria as surfaces optimizations, except for the  $5 \times 5 \times 5$  **k**-points grid as is in a previous work [32].

Vibrational frequencies related to adsorbed H atoms have been obtained within the harmonic approximation by explicit diagonalization of the Hessian block matrix involving only adsorbate coordinates. The corresponding matrix elements of the Hessian matrix are obtained as finite differences of 0.03 Å. The intensity of each normal mode has been obtained from the vibration corresponding dipole moment change normal to surface.

### 3. Results and discussion

In this section we describe the results for the systems of interest. To ease the discussion and better focus on the different calculated and predicted values, separate subsection are used.

#### 3.1. Hydrogen adsorption and dissociation

Figure 1 displays the ZPE energy profile for H<sub>2</sub> dissociation on the different Mo<sub>n</sub>C (001) studied surfaces including or not the vdW correction. Furthermore, Table 1 summarizes the reaction energy values ( $\Delta E$ ), and the H<sub>2</sub> dissociation ( $E_b$ ) and formation ( $E_{br}$ ) energy barriers. On Figure 2, the sketches of H<sub>2</sub> and 2H\* adsorptions, as well as of H<sub>2</sub> dissociation transition states (TS), are shown for calculations including vdW dispersion; the frequency analysis is shown on Table S1 of the Supplementary Material. It is worth mentioning that, except in the case of the  $\beta$ -Mo surface, and due to cancelling effects, results including vdW interactions are markedly different from those neglecting them. Therefore, to describe H<sub>2</sub> adsorption and dissociation on these surfaces, dispersion terms should be taken into account. The adsorption data of H<sub>2</sub> molecule and 1 H isolated atom are displayed on Table S2 and S3, respectively.

In the case of the  $\beta$ -Mo surface, both approaches describe the H<sub>2</sub> dissociation as an essentially spontaneous process. The H<sub>2</sub> adsorption energy presents a difference of 0.15 eV between calculations with or without vdW dispersion, and the same difference is found for the two adsorbed hydrogen atoms. Thus, the calculated energy barrier for the H<sub>2</sub> formation including or not dispersion is the same (1.20 eV). Therefore, these results indicate that vdW dispersion does not play particularly a crucial role on the H<sub>2</sub> energy profile on  $\beta$ -Mo, probably owing to the fact that the electronic interaction between  $\beta$ -Mo and H<sub>2</sub> molecule is already strong (-0.67 eV), and vdW dispersion is usually used for describing very weak interactions.



Regarding  $\beta$ -C surface, the calculations without vdW dispersion show a very weak interaction between  $H_2$  and  $\beta$ -C surface (-0.02 eV) and an energy barrier of 0.33 eV for the H-H bond cleavage. Therefore,  $H_2$  desorption is favored with respect to dissociation, and, consequently, these results would seem to indicate that the  $H_2$  dissociation—a necessary step for many hydrogenation processes—would only occur on the  $\beta$ -Mo termination. However, calculations explicitly including the vdW terms predict a physisorption state with an adsorption energy of -0.30 eV with an essentially zero barrier for dissociation, as in the case of the  $\beta$ -Mo surface. This computational result would then suggest that  $H_2$  dissociation is likely to occur on both surface terminations. Since in the case of the  $\beta$ -C surface the interaction with  $H_2$  is very weak, the inclusion of vdW terms becomes unavoidable. Similar conclusions were obtained for methane adsorption on the same surfaces [47]. Not unexpectedly, the adsorbate molecular geometry remains unchanged [16,47].

Another remarkable fact is the high exothermicity on  $H_2$  dissociation on  $\beta$ -C where calculations including or not dispersion predict the formation of strong C-H bonds (1.10 Å). Furthermore, the low coverage H adsorption on  $\beta$ -C surface also implies surface reconstruction, due to the displacement of the CH moieties from the initial position to the vicinal Hollow  $Mo^2$  sites. This C redistribution, which is observed in previous works with  $CO_2$  as an adsorbate [23], stabilizes the surface energy increasing the exothermicity of the H adsorption process. The energy difference between reconstructed and non-reconstructed surface after the H adsorption is around 0.8 eV. In the recent work of Wang *et al.* [28] this surface reconstruction was not reported and for this reason the adsorption energy of  $2H^*$  atoms on  $\beta$ -Mo was found to be favorable with respect the adsorption on  $\beta$ -C, opposite to present results.

Notice that the reverse process ( $H_2$  formation) would imply an energy barrier of 2.27 eV, due to the high stability of the formed C-H bonds. This fact also suggests that, in spite of the low energy barrier for  $H_2$  dissociation, the hydrogenation catalytic activity would be smaller since H adatoms are strongly bound to the surface. In comparison to  $H_2$  adsorption on hexagonal  $\alpha$ - $Mo_2C$  phase [58], the  $H_2$  dissociation was also to be very exothermic and involved very low energy barriers (0.34 eV at worst). All these works are in agreement with Brønsted-Evans-Polanyi relationships, *i.e.* the higher the reaction energy, the lower the energy barriers [59].

Finally, results concerning the  $\delta$ -MoC(001) surface are similar to those on  $\beta$ -C surface, where the exposure of surface C atoms seems to play a key role, rather than the particular surface Mo:C ratio. From Table 1 one readily sees that the energy barriers for H<sub>2</sub> dissociation are not affected by dispersion, being 0.60 and 0.64 eV, without and with dispersion, respectively. Note, however, that when neglecting dispersion, desorption becomes favored with respect to dissociation. This is not the case when accounting for dispersion, where dissociation is favored over desorption. Therefore, even for such a small and simple adsorbate, the effect of dispersion cannot be disregarded. We close this discussion by noting that the energy barrier for H<sub>2</sub> dissociation on the  $\delta$ -MoC (001) surface is of the order of the value reported on TiC(001) [60,61] and ZrC(001) [62] which have also a face centered cubic structure. This supports the effect of metal/C ratio on the catalyst activity, since the transition metal carbides with metal/C ratio of two present a higher activity than TMCs with a ratio of one [23,26].

In summary, vdW dispersion should be included when aiming at describing H<sub>2</sub> adsorption, dissociation, and H formation on the studied surfaces of Mo carbides, especially on  $\delta$ -MoC (001) and  $\beta$ -C, where the H<sub>2</sub>-surface interaction is especially weak.

### 3.2 Full coverage surface hydrogenation

From an experimental point of view, in order to carry out hydrogenation reactions, the amount of H<sub>2</sub> used is usually in excess [63,64]. Therefore, the catalyst surface is likely to be completely covered by H atoms and this situation needs to be considered as well. To this end, different coverages containing of 1, 2, 8, and 16 H adsorbed atoms on the (2×2) supercells have been tested. Note that this is slightly different from the situation studied by Wang *et al.* [28] where, on the same (2×2) supercells, up to 20 and 24 adsorbed H atoms were considered depending on the surface termination. In this work, we consider that a maximum coverage is reached by 16 adsorbed H atoms since the sequential H<sub>2</sub> dissociation steps necessarily need available surface active sites, and probably, higher energy barriers would be obtained for subsequent hydrogenation due to the fact that active sites would be already occupied by H atoms. The adsorption energy values *per* atom, listed on Table S4, indicate that the full coverage surface hydrogenation is favorable and shows that the adsorption energy *per* atom is practically

the same whether the adsorption process includes 8 or 16 H atoms above the supercell. The most noticeable variations are detected on  $\delta$ -MoC (001) surface.

Figure 3 displays most stable  $\beta$ -Mo<sub>2</sub>C structures after hydrogen adsorption at full coverage. In the case of the  $\beta$ -Mo surface, the H atoms occupy hollow Mo sites despite of the fact that on the co-adsorption of 2 and 8 H atoms, the most favorable site is the C<sub>2</sub> hollow [23], see Figure 2a, in agreement with Wang *et al.* [28]. Probably this variation is due to the distribution of sites in the supercell surface model;  $\beta$ -Mo surface contains 8 hollow C<sub>2</sub> and 16 hollow Mo sites. If the first 8 H atoms are adsorbed on hollow C<sub>2</sub>, the rest of 8 H atoms should be adsorbed on hollow Mo and/or hollow C<sub>1</sub>, increasing the H-H interaction owing to the H-H proximity. Nevertheless, the 16 H adsorption on Hollow Mo sites reduces this H-H interaction. On the other hand, C atoms at the second and fourth layer remain unchanged after  $\beta$ -Mo hydrogenation, and therefore, one can consider the C atoms in the same layer as equal by symmetry.

Regarding to the hydrogen adsorption on the  $\beta$ -C surface, the reconstruction detected at low coverages is also observed at 50% coverage (8 H atoms). This is because after the H adsorption the surface energy of the reconstructed  $\beta$ -C is  $\sim 0.7$  eV more stable than non-reconstructed surface, where the C displaced atoms are located on Hollow Mo<sup>2</sup> sites (see Figure S1). Nevertheless, tests at full coverage—see Figure S2—reveal that the most stable  $\beta$ -C surface is a non-reconstructed structure as one can see on Figure 3. The full coverage hydrogenation on  $\beta$ -C surface leads to two degenerate structures even though both involve top C sites. The difference in these two different structures is on the distribution of CH, CH<sub>2</sub>, and CH<sub>3</sub> groups; see Figure 3. Note also that structure *A* contains the three kind of possible moieties whereas on *B*, only CH and CH<sub>3</sub> are present. Structure *A* is slightly more stable ( $\sim 0.12$  eV) than *B* although the adsorption energy *per* H atom is practically the same. In comparison to the study of Wang *et al.* [28], the stepwise adsorption of H atoms used by these authors lead to a situation where the 16 H atoms are located on top of C atoms, leading to the formation of CH<sub>2</sub> moieties. In the present work, this structure is  $\sim 0.3$  eV less stable than the *A* structure and it has not been further considered. Geometries where only CH moieties are formed and the rest of H atoms are located on Hollow C and Mo sites, are  $\sim 2$  eV higher in energy (see Figure S2).

The particular distribution of H atoms implies that the environment around the surface C atoms is different and, consequently, the C(1s) CLBEs of these atoms could be different although whether the difference may be resolved remains an open question which we address in a forthcoming section. The difference in functionalized C atoms may also be visible by means of IR spectroscopy, considered later on. Besides, the different environment on C atoms located in the first atomic layer could also affect C atoms in the third layer. To facilitate the discussion, Figure 3 presents the notation employed to distinguish the C atoms at the first and third atomic layers. Different atoms in the first layer are described by numbers and those of the third layer by capital letters. Figure 4 displays full and half coverages of hydrogenated  $\delta$ -MoC(001) surface, where H atoms occupy top-C and top-Mo sites. In the case of full H coverage, from the eight C-H bond thus formed, only four involve a significant ( $\sim 1$  Å) displacement of the C atoms along the vacuum direction. The reason behind this surface rumpling is simply to decrease the vicinal H-H repulsion. To proof that this is the case, calculations have been carried out hampering these C displacements. In this artificial structure, the total energy is 2 eV higher. On the other hand, in the half coverage situation, H adsorption occurs only on top of C surface atoms. Note that the C surface rumpling is not as pronounced as compared to full coverage situation. Due to stability reasons commented in the next subsection, the 50% H covered system is the key surface hydrogenated model of  $\delta$ -MoC(001). Following the notation used for the  $\beta$ -C surface, the different surface C atoms of  $\delta$ -MoC(001) are denoted using numbers. In the fully relaxed situation, the symmetry of C atoms in the first atomic layer is broken and one may wonder whether the distinct C atoms can be distinguished. For instance, the different C atoms may exhibit sufficiently large  $\Delta$ CLBEs for the C(1s) which shall be also discussed later on.

### 3.3. Relative stability of H-covered $Mo_nC$ (001) surfaces

The largely exothermic adsorption energy values reported on Table S2 show that the presence of H atoms stabilize these surfaces. In the case of  $\delta$ -MoC (001), the strong interaction implies a considerable surface rumpling. Nevertheless, from the adsorption energy values only it is not possible to establish the relative stability of surfaces with different H coverage situations. To estimate the relative stability of H-covered  $\beta$ -C,  $\beta$ -Mo, and  $\delta$ -MoC (001) surfaces we rely on the calculated surface free energy of H covered ( $\gamma^{\text{cover}}$ ) following the *ab initio* atomistic thermodynamics formalism described

in the previous section and using values of hydrogen chemical potential ( $\Delta\mu_{0_{H_2}}$ ) at different working temperatures and pressures, and the pertinent surface free energy values.

Figure 5 reports the calculated adsorption free energy of the three studied surfaces respect to the H coverage at different temperatures setting the external pressure to 5 atm, used in the past for catalytic hydrogenation reactions [24,26]. The results for all temperatures, pressures, and coverage conditions considered in the present work are listed in Table S5. From Figure 5 one can first observe that increasing the temperature slightly destabilizes the surfaces. Note that for  $\beta$ -Mo<sub>2</sub>C, independently of the surface termination, the surface stability increases with increasing H coverage at working conditions [23,24,26].

From the preceding discussion this fact is not so unexpected since H atoms adsorption on this surface result in the formation of strong C-H bonds in the case of  $\beta$ -C surface, and, in the case of  $\beta$ -Mo, the charge transfer from Mo to H atoms stabilizes the system —see Table S6. A slightly different situation is found for the  $\delta$ -MoC (001) surface where it is stabilized up to half coverage, whereas further increasing of hydrogen coverage up to full coverage destabilizes the surface. This is simply because situation with H coverage higher than 50% involve H atoms at Mo sites; recall that H atoms are preferably bonded to C surface sites as observed on Table S3. Note that, on Table S6, the charge transfer from Mo to H is half with respect  $\beta$ -Mo.

Furthermore, the surface area is lower than on  $\beta$ -Mo<sub>2</sub>C, which probably implies a superior H-H repulsion at higher coverages. On Table S5 one can check that at all tested pressures and temperatures, the  $\gamma^{\text{cover}}$  at half coverage present the lower values, and consequently, the simulation of characterization techniques carried out in the next sections has been performed using the 50% of covered surface model for  $\delta$ -MoC and the full coverage model for  $\beta$ -Mo<sub>2</sub>C surfaces. Finally, on Figure S3, we display the Gibbs adsorption energy respect the pressure and temperature at the full coverage situation, where, for all tested surfaces, low temperatures and high pressures stabilize the full covered surfaces.

### *3.4. Analysis of the core level binding energy shifts*

Table 2 reports the calculated  $\Delta\text{CLBEs}$  values for the C(1s) on  $\beta\text{-Mo}$  surface obtained at the initial state approximation on the bare and fully hydrogenated situations. Since the chemical environment affect  $\Delta\text{CLBEs}$ , some structural data such as the C-H bond length have been added to the tables to provide geometric information about the origin of these shifts. Also, a comparison between calculations including or not the vdW terms reveal that the latter do not play any role on the calculated  $\Delta\text{CLBEs}$ , differences being a constant shift for each surface of at most 0.09 eV.

For clean surfaces, all atoms in a given atomic layer are symmetrically equivalent and, hence, one single  $\Delta\text{CLBE}$  value with respect to  $\text{Mo}_2\text{C}$  bulk is used for atoms in each atomic layer. For  $\beta\text{-Mo}$  surface,  $\Delta\text{CLBEs}$  for the C atoms located at fourth layer are not shown since this in principle bulk-like layer is artificially in contact with vacuum. Here,  $\Delta\text{CLBEs}$  for C atoms in the second layer are almost the same irrespective of the presence of adsorbed H atoms and, hence, within the limit of resolution even using synchrotron radiations which is  $\sim 0.1$  eV [65].

A different situation is found for  $\beta\text{-C}$  (Table 3), where even for the clean surface noticeable shifts are predicted which could be used to detect the presence of this termination. For the H-covered  $\beta\text{-C}$  surface, C-H bond formation leads to the noticeable  $\Delta\text{CLBEs}$  with respect to bulk, but not so large when compared to the bare surface. Nevertheless, the formed CH,  $\text{CH}_2$ , and  $\text{CH}_3$  like species have different  $\Delta\text{CLBEs}$  which could be detected by XPS. Within the initial state approximation, the  $\Delta\text{CLBEs}$  are negative. The larger shifts ( $\sim 1.1$  eV) correspond to the C-H species whereas the smaller shifts ( $\sim 0.40$  eV) corresponds to C bonded to three H atoms. The main difference between *A* and *B* geometries is the different  $\Delta\text{CLBEs}$  for  $\text{CH}_2$  species, which are not present on *B*. Eventually, one must take into account that both  $\beta\text{-Mo}$  and  $\beta\text{-C}$  terminations coexist and, unless using high resolution XPS,  $\Delta\text{CLBEs}$  implying rather broad XPS peaks could be observably precluding the unequivocal assignment to a particular surface termination.

The  $\Delta\text{CLBEs}$  values corresponding to the clean and half H-covered  $\delta\text{-MoC}(001)$  surface are listed on Table 4. For the bare surface,  $\Delta\text{CLBEs}$  calculated using the initial state approximation are close to the bulk for all relevant atomic layers. Upon hydrogenation, the  $\Delta\text{CLBEs}$  with respect to  $\delta\text{-MoC}$  bulk corresponding to C atoms

located in the first atomic layer are negative and values for different types of C atoms, with different displacements on  $z$  axis direction, are probably not sufficiently different to allow experimental identification. No noticeable  $\Delta$ CLBEs values are found for the C in deeper atomic layers.

### 3.6. Infrared spectra

In order to provide information that can be used in eventual experiments using IR spectroscopies, simulated IR spectra of each of the studied surfaces have been obtained. Figure 6 reports all calculated spectra with those corresponding to the bare surface displayed on the left panels, and the fully hydrogenated surfaces on the right panels. In the view of all preceding results, simulated IR spectra have been obtained only without vdW dispersion. Let us to analyze the results in Figure 6 in some detail. For the bare surfaces, one can distinguish peaks below to  $1000\text{ cm}^{-1}$  region typically observed with Raman spectroscopies. More specifically, Mo related vibrations are located below  $300\text{ cm}^{-1}$  whereas C related ones appear around  $400\text{-}600\text{ cm}^{-1}$ . For the hydrogenated surfaces, one can observe small differences on the bare surface vibrations zone, probably, due to coupling to H related vibrational modes. The most remarkable peaks on  $\delta$ -MoC (001) surface are the C-H symmetric ( $\nu_s$ ) and asymmetric stretching ( $\nu_a$ ) vibrations located at  $2838$  and  $2824\text{ cm}^{-1}$ , respectively. Taking into account the obtained results on the previous sections, the half covered surface is the most stable after H adsorption, without H atoms adsorbed on Mo surface atoms. However, the improbable adsorption of some H atoms on top Mo site could be detected by IR spectroscopy since, as one can see on Figure S4 on the Supplementary Material, the Mo-H asymmetric stretching ( $\nu_a$ ) appears at  $\sim 1730\text{ cm}^{-1}$  while the symmetric one ( $\nu_s$ ) at  $\sim 1755\text{ cm}^{-1}$ .

Logically, in the case of the  $\beta$ -Mo surface (Figure 6b), the C-H stretching is not observed since H occupies hollow Mo atoms. This implies that Mo-H  $\nu_s$  appears at  $\sim 1030\text{ cm}^{-1}$  and the  $\nu_a$  at  $\sim 1100\text{ cm}^{-1}$ . These different bonding situations respect the possible (and improbable) adsorption of H atoms on  $\delta$ -MoC (001) would be easily observed by IR experiments. At this surface, H bending ( $\delta$ ) is predicted to appear at around  $750\text{-}900\text{ cm}^{-1}$ . On the  $\beta$ -C surface, the simulated IR spectra for both degenerate  $A$  and  $B$  structures have been performed. As one can see from Figure 6c and 6d, the spectra are very similar with a clear feature at  $1176\text{ cm}^{-1}$  corresponding to the  $\text{CH}_3$   $\nu_s$ . Furthermore, the C-H  $\nu_s$  and  $\nu_a$  of  $\text{CH}_3$  surface species would appear at  $2700\text{-}2900\text{ cm}^{-1}$ .

for both surface structures, yet with weak intensities. Finally, there are also slight differences such as the C-Mo stretching on C atoms bonded to one H, detected on geometry *B* at  $\sim 970\text{ cm}^{-1}$ , or the CH<sub>2</sub> moieties in geometry *A*, with a peak around 450-550  $\text{cm}^{-1}$  corresponding to CH<sub>2</sub> twisting ( $\tau$ ), whereas on structure *B* there are no peaks at this region. Clearly, IR could provide information regarding the surface hydrogenation state.

#### 4. Conclusions

Here an extensive theoretical study of the adsorption, dissociation, and formation of H<sub>2</sub> on cubic  $\delta$ -MoC and orthorhombic  $\beta$ -Mo<sub>2</sub>C (001) surfaces —the last one with C and Mo terminations— has been carried out at DFT level using the PBE functional including or not dispersion terms.

Results show that the energy profiles for the H<sub>2</sub> dissociation elementary steps are largely affected by dispersion. The calculations with vdW present an energy barrier essentially zero on  $\beta$ -Mo and  $\beta$ -C, and of 0.60 eV for  $\delta$ -MoC, whereas calculations without vdW predict that on  $\beta$ -C and  $\delta$ -MoC desorption would be more favorable than dissociation. The present calculations at low H coverage predict that for the three studied surfaces, H<sub>2</sub> dissociation is strongly exothermic, favoring dissociation against recombination. Taking into account the adsorption of one H<sub>2</sub> molecule on the (2 $\times$ 2) supercell,  $\beta$ -Mo<sub>2</sub>C presents an essentially zero energy barrier for the H<sub>2</sub> dissociation, whilst the most appropriate for H<sub>2</sub> formation is  $\delta$ -MoC. Surface free energy calculations reveal that both terminations of  $\beta$ -Mo<sub>2</sub>C are stabilized with increasing H coverage. However, in the case of the  $\delta$ -MoC (001) surface, H adsorption stabilizes up to half coverage where all C sites are occupied.

Regarding the simulation of properties which could be observed by means of usual surface characterization techniques, both XPS and IR are able to provide details of the surface structure before and after H deposition. The initial state core level binding energy shifts for C 1s indicate that it would be possible to distinguish many different environments around C atoms, such as CH, CH<sub>2</sub>, and CH<sub>3</sub> moieties on  $\beta$ -C surface or the different C rumpling on  $\delta$ -MoC triggered by C-H bond formation. Other minor changes have been detected through computational tools although these variations are below the resolution of XPS using synchrotron (0.1 eV). The different moieties



produced after H adsorption—  $\text{CH}_3$  ( $\beta$ -C) or  $\text{CH}$  ( $\beta$ -C and  $\delta$ -MoC)— as well as the different H adsorption sites could be distinguished by means of IR experiments.

## Acknowledgements

This manuscript has been authored by employees of Brookhaven Science Associates, LLC under Contract No. DE-SC0012704 with the U.S. Department of Energy. The research carried out at the *Universitat de Barcelona* was supported by the Spanish MINECO/FEDER grant CTQ2015-64618-R, and, in part, by *Generalitat de Catalunya* (grants 2014SGR97 and XRQTC) and from the NOMAD Center of Excellence project; the latter project has received funding from the European Union Horizon 2020 research and innovation programme under grant agreement N° 676580. S.P.P. acknowledges financial support from Spanish MEC predoctoral grant associated to CTQ2012-30751. F.V. thanks the MINECO for his postdoctoral *Ramón y Cajal* (RyC) research contract (RYC-2012-10129) and F.I. acknowledges additional support from the 2015 ICREA Academia Award for Excellence in University Research. Computational time at the *MARENOSTRUM* supercomputer has been provided by the Barcelona Supercomputing Centre (BSC) through a grant from *Red Española de Supercomputación* (RES).

**Table 1:** H<sub>2</sub> adsorption energy ( $E_{\text{ads}}$ ), dissociation energy ( $\Delta E$ ), dissociation energy barrier ( $E_b$ ), and H<sub>2</sub> formation energy barrier ( $E_{\text{rb}}$ ), including vdW dispersion or not, on  $\beta$ -Mo,  $\beta$ -C, and  $\delta$ -MoC (001) surfaces. All energies are given in eV.

Non-vdW					vdW			
	$E_{\text{ads}}$	$\Delta E$	$E_b$	$E_{\text{rb}}$	$E_{\text{ads}}$	$\Delta E$	$E_b$	$E_{\text{rb}}$
$\beta$ -Mo	-0.67	-1.20	$\sim 0$	1.20	-0.82	-1.20	$\sim 0$	1.20
$\beta$ -C	-0.02	-2.31	0.32	2.63	-0.30	-2.26	$\sim 0$	2.27
$\delta$ -MoC	-0.46	-0.11	0.64	0.75	-0.70	-0.35	0.60	0.96

**Table 2:** Core level binding energy shifts ( $\Delta\text{CLBEs}$ ) for C( $1s$ ) on bare ( $\Delta\text{CLBE}^b$ ) and fully hydrogenated ( $\Delta\text{CLBE}^H$ ) situations for the  $\beta$ -Mo surface using the initial state approximation. The results are separated depending on whether vdW dispersion is included or not. All shifts are given in eV.

	Non-vdW		vdW	
	$\Delta\text{CLBE}^b$	$\Delta\text{CLBE}^H$	$\Delta\text{CLBE}^b$	$\Delta\text{CLBE}^H$
$2^{\text{nd}}$ layer	-0.08	-0.21	-0.10	-0.24

**Table 3:** Core level binding energy shifts ( $\Delta\text{CLBEs}$ ) for C(1s) on bare ( $\Delta\text{CLBE}^b$ ) and fully hydrogenated ( $\Delta\text{CLBE}^H$ ) situations for the  $\beta\text{-C}$  surface using the initial state approximation. The results are separate depending on whether vdW dispersion is included or not. All shifts are given in eV. The C-H bond length,  $d(\text{C-H})$ , in Å, has been included to distinguish the different moieties and the bonding differences. The C nomenclature is as in Figure 2. *A* and *B* correspond to the two different structures compatible with full coverage.

	No vdW				vdW			
	$\Delta\text{CLBE}^b$	$\Delta\text{CLBE}^H$	Moiety	d (C-H)	$\Delta\text{CLBE}^b$	$\Delta\text{CLBE}^H$	Moiety	d (C-H)
<b>Geometry A</b>								
1 <sup>st</sup> layer								
C <sup>1</sup>	-0.71	-1.03	CH	1.11	-0.74	-1.05	CH	1.10
C <sup>2</sup>		-0.43	CH <sub>3</sub>	1.11/1.12/1.12		-0.41	CH <sub>3</sub>	1.11/1.12/1.12
C <sup>3</sup>		-1.03	CH	1.11		-1.05	CH	1.10
C <sup>4</sup>		-0.43	CH <sub>3</sub>	1.11/1.12/1.12		-0.41	CH <sub>3</sub>	1.11/1.12/1.12
C <sup>5</sup>		-0.51	CH <sub>2</sub>	1.10/1.18		-0.55	CH <sub>2</sub>	1.10/1.18
C <sup>6</sup>		-0.74	CH <sub>2</sub>	1.10/1.18		-0.77	CH <sub>2</sub>	1.10/1.17
C <sup>7</sup>		-0.51	CH <sub>2</sub>	1.10/1.18		-0.55	CH <sub>2</sub>	1.10/1.18
C <sup>8</sup>		-0.73	CH <sub>2</sub>	1.10/1.18		-0.77	CH <sub>2</sub>	1.10/1.17
3 <sup>rd</sup> layer								
C <sup>A</sup>	-0.09	-0.13	-	-	-0.10	-0.13	-	-
C <sup>B</sup>		-0.11	-	-		-0.11	-	-
C <sup>C</sup>		-0.13	-	-		-0.13	-	-
C <sup>D</sup>		-0.11	-	-		-0.11	-	-
C <sup>E</sup>		-0.13	-	-		-0.14	-	-
C <sup>F</sup>		-0.18	-	-		-0.18	-	-
C <sup>G</sup>		-0.13	-	-		-0.14	-	-
C <sup>H</sup>		-0.18	-	-		-0.18	-	-
<b>Geometry B</b>								
1 <sup>st</sup> layer								
C <sup>1</sup>	-0.71	-1.10	CH	1.10	-0.74	-1.12	CH	1.11
C <sup>2</sup>		-0.40	CH <sub>3</sub>	1.11/1.12/1.13		-0.38	CH <sub>3</sub>	1.11/1.12/1.13
C <sup>3</sup>		-1.10	CH	1.10		-1.12	CH	1.11
C <sup>4</sup>		-0.40	CH <sub>3</sub>	1.11/1.12/1.13		-0.38	CH <sub>3</sub>	1.11/1.12/1.13
C <sup>5</sup>		-0.45	CH <sub>3</sub>	1.11/1.12/1.12		-0.44	CH <sub>3</sub>	1.11/1.12/1.12
C <sup>6</sup>		-0.93	CH	1.14		-0.95	CH	1.14
C <sup>7</sup>		-0.44	CH <sub>3</sub>	1.11/1.12/1.13		-0.44	CH <sub>3</sub>	1.11/1.12/1.13
C <sup>8</sup>		-0.92	CH	1.14		-0.94	CH	1.14
3 <sup>rd</sup> layer								
C <sup>A</sup>	-0.09	-0.22	-	-	-0.10	-0.22	-	-
C <sup>B</sup>		-0.13	-	-		-0.14	-	-
C <sup>C</sup>		-0.22	-	-		-0.23	-	-
C <sup>D</sup>		-0.13	-	-		-0.13	-	-
C <sup>E</sup>		-0.13	-	-		-0.14	-	-
C <sup>F</sup>		-0.24	-	-		-0.25	-	-
C <sup>G</sup>		-0.14	-	-		-0.14	-	-
C <sup>H</sup>		-0.24	-	-		-0.25	-	-

**Table 4:** Core level binding energy shifts ( $\Delta\text{CLBEs}$ ) for C(1s) on bare ( $\Delta\text{CLBE}^b$ ) and hydrogenated ( $\Delta\text{CLBE}^H$ ) for the  $\delta\text{-MoC}(001)$  surface using the initial state approximation. The results are separate depending on whether vdW dispersion is included or not. All shifts are given in eV. For comparison, C-H and C-Mo bond lengths,  $d(\text{C-H})$  and  $d(\text{C-Mo}^2)$ , respectively, both in Å, are also reported. The C nomenclature is referred to Figure 3.

	No vdW				vdW			
	$\Delta\text{CLBE}^b$	$\Delta\text{CLBE}^H$	$d(\text{C-H})$	$d(\text{C-Mo}^2)$	$\Delta\text{CLBE}^b$	$\Delta\text{CLBE}^H$	$d(\text{C-H})$	$d(\text{C-Mo}^2)$
Initial State								
1 <sup>st</sup> layer	-0.14				-0.14			
C <sup>1</sup>		-0.42	1.11	2.30		-0.42	1.12	2.31
C <sup>2</sup>		-0.66	1.12	2.65		-0.66	1.12	2.65
C <sup>3</sup>		-0.42	1.11	2.31		-0.42	1.12	2.31
C <sup>4</sup>		-0.67	1.12	2.65		-0.67	1.12	2.65
C <sup>5</sup>		-0.72	1.12	2.85		-0.72	1.12	2.85
C <sup>6</sup>		-0.67	1.12	2.68		-0.67	1.12	2.67
C <sup>7</sup>		-0.73	1.12	2.85		-0.73	1.12	2.85
C <sup>8</sup>		-0.67	1.12	2.67		-0.67	1.12	2.67
2 <sup>nd</sup> layer	0.08	-0.17	-	-	0.08	-0.17	-	-
3 <sup>rd</sup> layer	0.20	0.25	-	-	0.20	0.25	-	-

**Figure 1:** Energy profile of  $H_2$  adsorption and dissociation including ZPE correction on  $\beta$ -Mo,  $\beta$ -C, and  $\delta$ -MoC (001) surfaces including vdW terms (dashed lines) or not (solid lines).

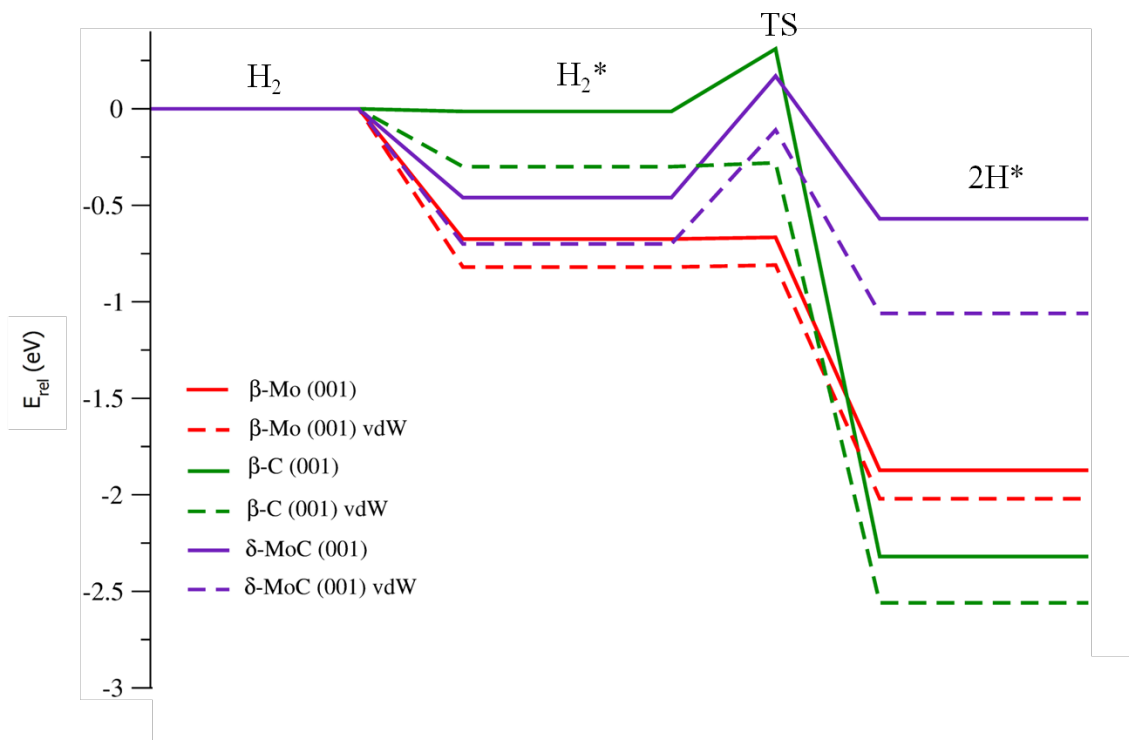


**Figure 2:** Sketches on side view (top) and top view (bottom) of  $H_2$  adsorption (left), TS (middle), and  $2H^*$  adsorption (right) on  $\beta$ -Mo (a),  $\beta$ -C (b), and  $\delta$ -MoC (c) (001) surfaces. Pictures correspond to calculations including vdW dispersion. Violet, green, and white balls represents Mo, C, and H atoms, respectively.

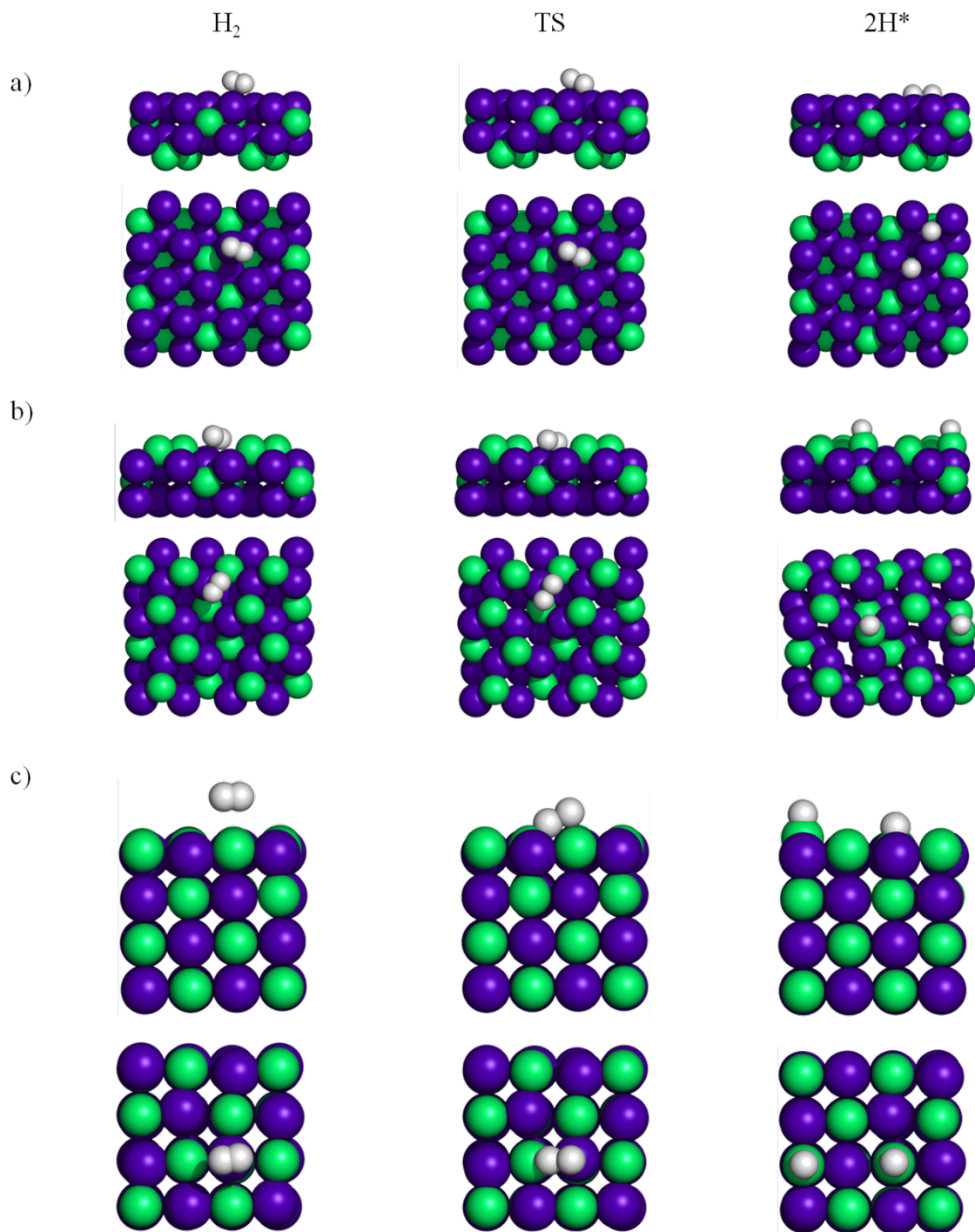


**Figure 3:** Sketches on top view of full coverage hydrogenated  $\beta$ -Mo and  $\beta$ -C —two degenerate structures. For  $\beta$ -C surface one can see the nomenclature of C atoms used on Table 3. Sphere coloring as in Figure 2.

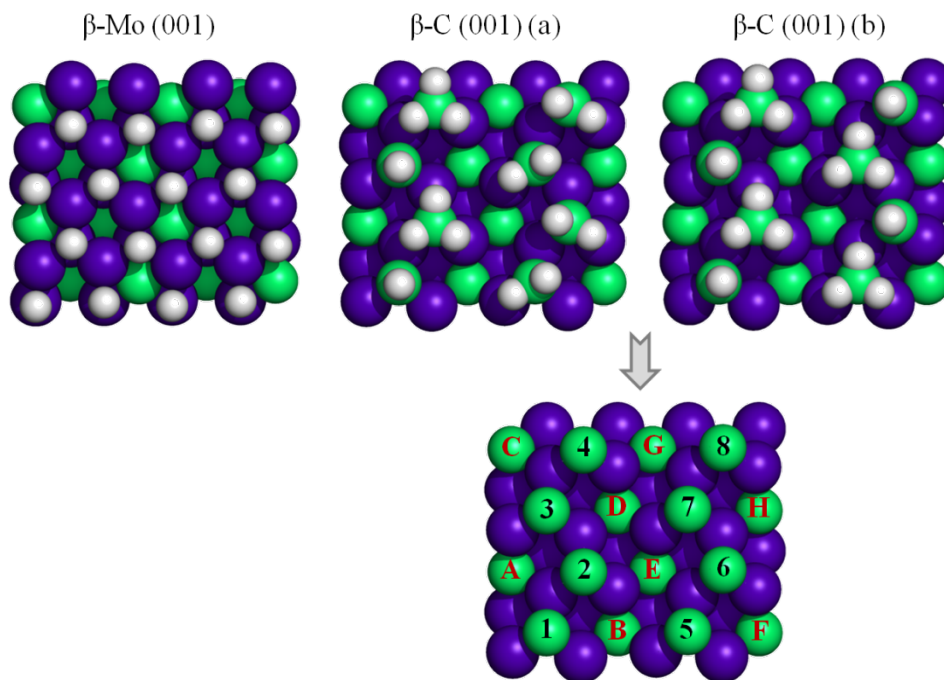




**Figure 4:** Sketches on side view (top) and top view (bottom) of full coverage (a) and half coverage (b) hydrogenated  $\delta$ -MoC (001) surface. Picture (c) shows the C surface nomenclature of 50% hydrogenated surface used on Table 4. Sphere coloring as in Figure 2.

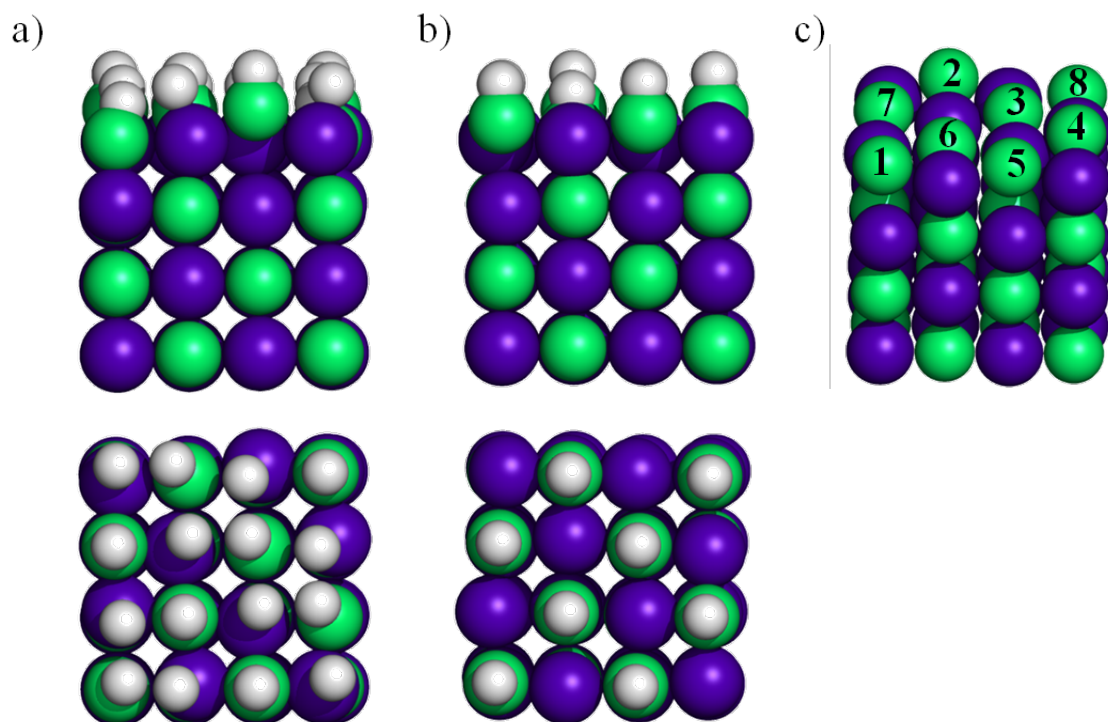


**Figure 5:** Plots of surface free energy at H coverage ( $\gamma^{\text{cover}}$ ) depending of the temperature at different H coverage at 5 atm of pressure.

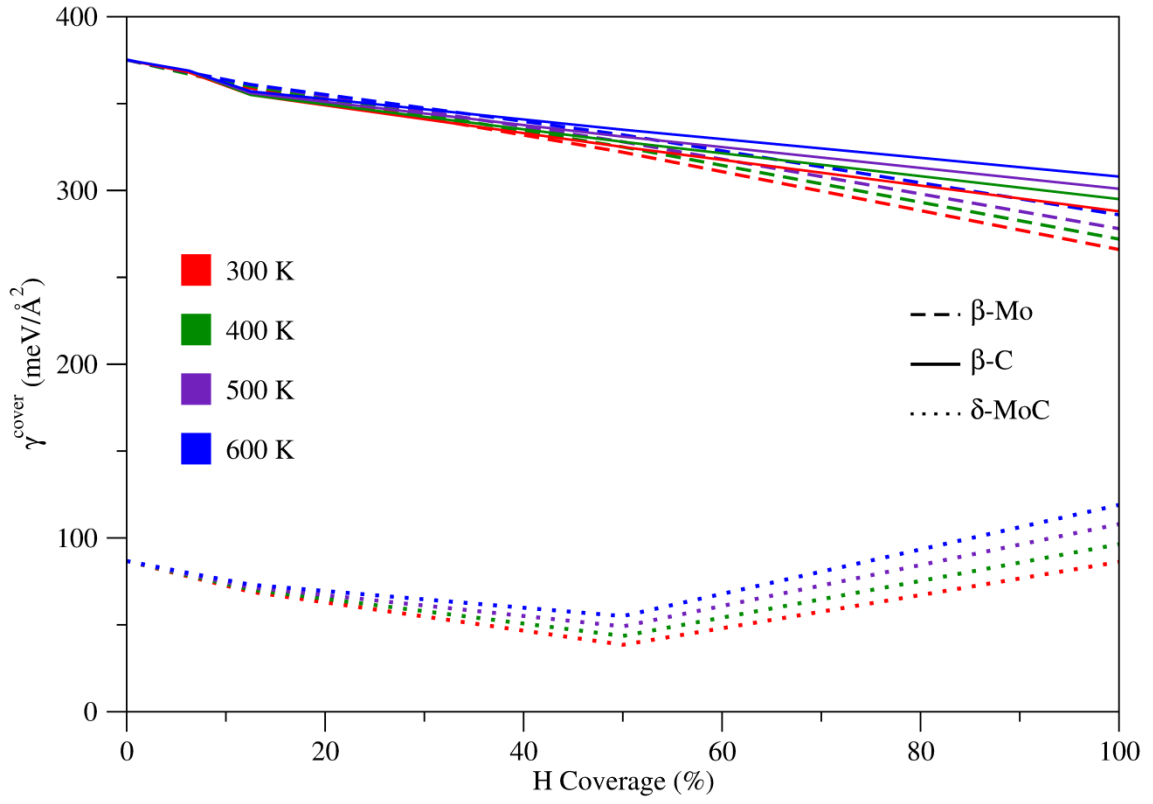
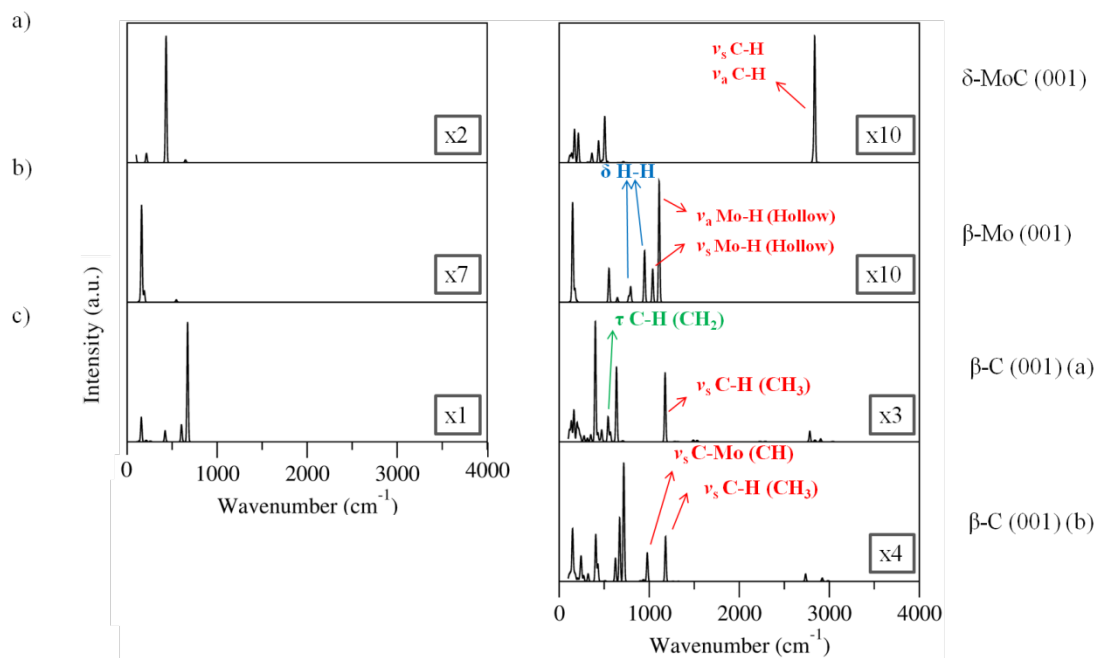


**Figure 6:** Simulated IR spectra of bare (left) and fully hydrogenated, full coverage, (right) of  $\delta$ -MoC (a),  $\beta$ -Mo (b), and  $\beta$ -C (c) (001) surfaces. The intensities have been enlarged by factor shown on the respective panels in order to improve the visualization.



## References

---

- [1] R. B. Levy, M. Boudart, *Science* 181 (1973) 547.
- [2] H.H. Hwu, G. Chen, *Chem. Rev.* 105 (2005) 185.
- [3] A.L. Stottlemeyer, T.G. Kelly, Q. Meng, J.G. Chen, *Surf. Sci. Rep.* 67 (2012) 201.
- [4] M.D. Porosoff, X. Yang, J.G. Chen, *Energy Environ. Sci.* 9 (2016) 62.
- [5] M.M. Sullivan, C.J. Chen, A. Bhan, *Catal. Sci. Technol.* 6 (2016) 602.
- [6] J.G. Chen, *Surf. Sci. Rep.* 30 (1997) 1.
- [7] J.G. Chen, *Chem. Rev.* 96 (1996) 1477.
- [8] S.T. Hunt, M. Milina, A.C. Alba-Rubio, C.H. Hendon, J.A. Dumesic, Y. Román-Leshkov, *Science* 352 (2016) 974.
- [9] Y. N. Regmi, G. R. Waetzig, K. D. Duffee, S. M. Schmuecker, J. M. Thode, B. M. Leonard, *J. Mater. Chem. A*, 3 (2015) 10085.
- [10] J.J. Liao, R.C. Wilcox, R.H. Zee, *Scripta. Metall. Mater.* 24 (1990) 1647.
- [11] J.A. Nelson, M.J. Wagner, *Chem. Mater.* 14 (2002) 4460.
- [12] M.D. Porosoff, M.N.Z. Myint, S. Kattel, Z. Xie, E. Gomez, P. Liu, J.G. Chen, *Angew. Chem. Int. Ed.* 54 (2015) 15501.
- [13] J.A. Rodriguez, P. Liu, Y. Takahashi, K. Nakamura, F. Viñes, F. Illas, *J. Am. Chem. Soc.* 131 (2009) 8595.
- [14] J.A. Rodriguez, P.J. Ramírez, G.G. Asara, F. Viñes, J. Evans, P. Liu, J.M. Ricart, F. Illas, *Angew. Chem. Int. Ed.* 53 (2014) 11270.
- [15] T.P. Saint Clair, S.T. Oyama, D.F. Cox, S. Otani, Y. Ishizawa, R.L. Low, K. Fukui, Y. Iwasawa, *Surf. Sci.* 426 (1999) 187.
- [16] C. Jimenez-Orozco, E. Florez, A. Moreno, P. Liu, J.A. Rodriguez, *J. Phys. Chem. C* 120 (2016) 13531.
- [17] P. Liu, J.A. Rodriguez, *J. Phys. Chem. B* 110 (2006) 19418.
- [18] N.M. Schweitzer, J.A. Schaidle, O.K. Ezekoye, X. Pan, S. Linic, L.T. Thompson, *J. Am. Chem. Soc.* 133 (2011) 2378.

- 
- [19] Y. Liu, J. Ding, J. Sun, J. Zhang, J. Bi, K. Liu, F. Kong, H. Xiao, Y. Sun, J. Chen, *Chem. Commun.* 52 (2016) 5030.
- [20] Y. Shi, Y. Yang, Y.W. Li, H. Jiao, *Catal. Sci. Technol.* 6 (2016) 4923.
- [21] R. Barthos, F. Solymosi, *J. Catal.* 249 (2007) 289.
- [22] M.D. Porosoff, X. Yang, J.A. Boscoboinik, J.G. Chen, *Angew. Chem. Int. Ed.* 53 (2014) 6705.
- [23] S. Posada-Pérez, F. Viñes, P.J. Ramirez, A.B. Vidal, J.A. Rodriguez, F. Illas, *Phys. Chem. Chem. Phys.* 16 (2014) 14912.
- [24] S. Posada-Pérez, P.J. Ramirez, R.A. Gutierrez, D.J. Stacchiola, F. Viñes, P. Liu, F. Illas, J.A. Rodriguez, *Catal. Sci. Technol.* DOI: 10.1039/c5cy02143j.
- [25] L. Li, D.S. Sholl, *ACS. Catal.* 5 (2015) 5174.
- [26] S. Posada-Pérez, P.J. Ramírez, J. Evans, F. Viñes, P. Liu, F. Illas, J.A. Rodríguez, *J. Am. Chem. Soc.* 138 (2016) 8269.
- [27] A. Vojvodic, *Catal. Lett.* 142 (2012) 728.
- [28] T. Wang, X. Tian, Y. Yang, Y.W. Li, J. Wang, M. Beller, H. Jiao, *Surf. Sci.* 651 (2016) 195.
- [29] K. Reuter, M. Scheffler, *Phys. Rev. B*, 65 (2002) 035406.
- [30] K. Reuter, M. Scheffler, *Phys. Rev. Lett.* 90 (2003) 046103.
- [31] Powder Diffraction File; JCPDS International Center for Diffraction Data: Pennsylvania, 2004.
- [32] J.R.d.S. Politi, F. Viñes, J. A. Rodriguez, F. Illas, *Phys. Chem. Chem. Phys.* 15 (2013) 12617.
- [33] J.W. Han, L.W. Li, D.S. Sholl, *J. Phys. Chem. C* 115 (2011) 6870.
- [34] J. Ren, C.-F. Huo, J. Wang, Z. Cao, Y.-W. Li, H. Jiao, *Surf. Sci.* 600 (2006) 2329.
- [35] H. Tominaga, Y. Aoki, M. Nagai, *Appl. Catal. A* 423–424 (2012) 192.
- [36] H. Tominaga, M. Nagai, *J. Phys. Chem. B* 109 (2005) 20415.
- [37] A.N. Christensen, *Acta Chem. Scand. Ser. A* 31 (1977) 509.

- 
- [38] E. Parthé, V. Sadagopan, *Acta Crystallogr.* 16 (1963) 202.
- [39] J.P. Perdew, K. Burke, M. Ernzerhof, *Phys. Rev. Lett.* 77 (1996) 3865.
- [40] S. Grimme, *J. Comput. Chem.* 27 (2006) 1787.
- [41] P.E. Blöchl, *Phys. Rev. B* 50 (1994) 17953.
- [42] G. Kresse, D. Joubert, *Phys. Rev. B* 59 (1999) 1758.
- [43] H.J. Monkhorst, J.D. Pack, *Phys. Rev. B: Solid State* 13 (1976) 5188.
- [44] G. Henkelman, H. Jonsson, *J. Chem. Phys.* 111 (1999) 7010.
- [45] F. Viñes, A. Iglesias-Juez, F. Illas, M. Fernández-García, *J. Phys. Chem. C* 118 (2014) 1492.
- [46] G. Kresse, J. Hafner, *Phys. Rev. B* 47 (1993) 558.
- [47] S. Posada-Pérez, J.R.d.S. Politi, F. Viñes, F. Illas, *RSC Adv.* 5 (2015) 33737.
- [48] T. Wang, X. Liu, S. Wang, C. Huo, Y.W. Li, J. Wang, H. Jiao, *J. Phys. Chem. C* 115 (2011) 22360.
- [49] N.H. Moreira, G. Dolgonos, B. Aradi, A.L. da Rosa, T. Frauenheim, *J. Chem. Theory. Comput.* 5, (2009) 605.
- [50] C.G. Tang, M.J.S. Spencer, A. S. Barnard, *Phys. Chem. Chem. Phys.* 16 (2014) 22139.
- [51] P.S. Bagus, *Phys. Rev.* 139 (1965) A619.
- [52] P.S. Bagus, E.S. Ilton, C.J. Nelin, *Surf. Sci. Rep.* 68 (2013) 273.
- [53] P.S. Bagus, F. Illas, G. Pacchioni, F.J. Parmigiani, *Electron. Spectrosc. Relat. Phenom.* 100 (1999) 215.
- [54] D.P. Chong, E.J. Gritsenko, E.J. Baerends, *J. Chem. Phys.* 116 (2002) 1760.
- [55] M. Segala, Y. Takahata, D.P. Chong, *J. Electron Spectrosc. Relat. Phenom.* 151 (2006) 9.
- [56] N. Pueyo-Bellafont, P.S. Bagus, F. Illas, *J. Chem. Phys.* 142 (2015) 214102.
- [57] L. Köhler, G. Kresse, *Phys. Rev. B* 70 (2004) 165405.

- 
- [58] T. Wang, Y.W. Li, J. Wang, M. Beller, H. Jiao, J. Phys. Chem. C 118 (2014) 8079.
- [59] F. Viñes, A. Vojvodic, F. Abild-Pedersen, F. Illas, J. Phys. Chem. C 117 (2013) 4168.
- [60] S. Posada-Pérez, F. Viñes, J.A. Rodriguez, F. Illas, Top. Catal. 58 (2015) 159.
- [61] F. Viñes, J.A. Rodriguez, P. Liu, F. Illas, J Catal. 260 (2008) 103
- [62] E. Florez, T Gomez, J.A. Rodriguez, F. Illas Phys. Chem. Chem. Phys. 13 (2011) 6865.
- [63] S.D. Senanayake, P.J. Ramírez, I. Waluyo, S. Kundu, K. Musiyanselage, Z. Liu, Z. Liu, S. Axnanda, D.J. Stacchiola, J. Evans, J. A. Rodriguez, J. Phys. Chem. C 120 (2016) 1778.
- [64] J. A. Rodriguez, J. Evans, L. Feria, A. B. Vidal, P. Liu, K. Nakamura, F. Illas, J. Catal. 307 (2013) 162.
- [65] A. Baraldi, J. Phys.: Condens. Matter 320 (2008) 86.